

## Reservoir Assessment Tool 2.0: Stakeholder driven improvements to satellite remote sensing based reservoir monitoring

Pritam Das<sup>a,\*</sup>, Faisal Hossain<sup>a</sup>, Shahzaib Khan<sup>a</sup>, Nishan Kumar Biswas<sup>b</sup>, Hyongki Lee<sup>c</sup>, Thanapon Piman<sup>d,f</sup>, Chinaporn Meechaiya<sup>e</sup>, Uttam Ghimire<sup>d</sup>, Kamal Hosen<sup>e</sup>

<sup>a</sup> Department of Civil and Environmental Engineering, University of Washington, Seattle, WA, USA

<sup>b</sup> Hydrological Sciences Laboratory, NASA Goddard Space Flight Center, Greenbelt, MD, USA

<sup>c</sup> Department of Civil and Environmental Engineering, University of Houston, Houston, TX, USA

<sup>d</sup> Stockholm Environment Institute, Bangkok, Thailand

<sup>e</sup> Asian Disaster Preparedness Center, Bangkok, 10400, Thailand

<sup>f</sup> Environmental Research Institute Chulalongkorn University, Bangkok, 10330, Thailand

### ARTICLE INFO

#### Keywords:

Reservoirs  
River regulation  
Satellites  
Stakeholder engagement

### ABSTRACT

In light of the rapidly increasing regulation of rivers due to planned and constructed reservoirs, monitoring reservoir operations has become very crucial. The Reservoir Assessment Tool (RAT) framework was developed to monitor reservoir operations globally, using hydrological modeling and satellite observations. With feedback from stakeholders, improvements in the RAT framework are demonstrated in this study using the Mekong River Basin as an example. A novel multi-sensor reservoir area mapping technique was developed using complementary strengths of optical and SAR sensors at a 1–5 day temporal resolution, allowing the quantification of sub-weekly reservoir operations. Additionally, the skill of radar altimeters in the RAT framework was tested using the Jason-3 altimeter. Using in-situ data from three Thai reservoirs in the Mekong Basin, consistent improvements were observed as compared to the original RAT framework. A functionality for visualizing forecasted outflow was also added using historically inferred reservoir operations or stakeholder-driven target storage expectations.

### 1. Introduction

Humans have significantly changed how the world's rivers flow by building dams and reservoirs at an unprecedented rate in the past couple of decades. Estimates suggest that about 1/6th of the total annual river flow is stored in reservoirs (Hanasaki et al., 2006; Mulligan et al., 2020). These reservoirs account for 57% of the Earth's total surface water storage variability (Cooley et al., 2021) that also have a characteristically different storage change pattern as compared to natural lakes (Ryan et al., 2020). These dams have significantly changed the seasonal streamflow characteristics of major rivers around the world (Cooley et al., 2021; Lehner et al., 2011; Zhou et al., 2016). For instance, due to regulation by existing reservoirs, the wet-season flow of the Mekong River is estimated to have reduced by 31%, while the dry-season flow has increased by 35% (Bonnema and Hossain, 2017; Mekong River Commission, 2019, 2021).

At a global scale, 48% of freshwater in rivers are impacted by

anthropogenic regulation due to reservoirs, which is projected to increase to about 93% in the future (Grill et al., 2015). The effects of this regulation are very apparent in the basin-wide disturbance to biodiversity (Barbarossa et al., 2020), sediment and nutrient flux to the oceans (Li et al., 2021), channel morphology and land-use-land-cover (Fernandes et al., 2020). Information on reservoir operations is therefore crucial to understand how streamflow regulation Drives human alteration of the natural aquatic environment and water resources. Developing this understanding requires prediction of the dynamic condition of the reservoir, such as inflow, outflow, active storage, storage change, water level and evaporative losses. Such data are usually measured and collected at the specific dam sites. However, barring a few exceptions, most data are not made publicly accessible or available, especially in developing nations, due to confidentiality requirements on grounds of national security (Plengsaeng et al., 2014) or lack of in-situ measurement infrastructure (Bernauer and Böhmelt, 2020; Bonnema and Hossain, 2017). Thus, the overwhelmingly opaque nature of dam

\* Corresponding author.

E-mail address: [pdas47@uw.edu](mailto:pdas47@uw.edu) (P. Das).

operations at most locations worldwide poses a significant challenge to tracking the dynamic nature of human alteration of flow by dams. Consequently, this hampers building a more complete understanding of the dam's impact on the natural-socioeconomic systems that are dependent on the river basins. This also hinders our ability to improve existing resource management tools in an increasingly dammed and human-impacted river basin in the future.

In dammed river basins, an increasing amount of a river's downstream streamflow is affected by upstream regulation. It is therefore crucial for these downstream reservoir operators to understand how the upstream reservoirs are operated, so that improved operating strategies can be adapted for irrigation, hydropower, and flood/drought management, while also maintaining environmental flow requirements (Bonnema et al., 2016). This naturally calls for cooperation and a need for open data-sharing among all dam operating and stakeholder agencies in a basin. However, this is difficult to establish and maintain in transboundary river basins (Bakker, 2009). Effective data sharing between countries requires a combination of various favorable factors, both technological and political (Balthrop and Hossain, 2010; Eldardiry and Hossain, 2021b). These include, but are not limited to, streamlined data-sharing mechanisms, transboundary water treaties for data sharing that facilitate reservoir operations and a willingness for all riparian countries to adopt a shared vision of development. Even in basins that are within a single country, such cooperation and data sharing can be a challenge. A prime example of which is the Cauvery basin dispute between the Indian states of Karnataka and Tamil Nadu (Khandekar and Srinivasan, 2021).

In this increasingly regulated and impounded river basin scenario of the near future, satellite remote sensing-based approaches can help fill the current gaps in data-availability and data access on reservoir operations and streamflow regulation. For instance, Global Reservoirs and Lakes Monitor (G-REALM; [https://ipad.fas.usda.gov/cropexplorer/global\\_reservoir/](https://ipad.fas.usda.gov/cropexplorer/global_reservoir/)) is one such satellite observation enabled product that reports the water level of select lakes and reservoirs based on satellite radar altimetry (Birkett et al., 2018). While such information on the water level of lakes and reservoirs can help understand the state of these water storage systems, additional information such as storage change, outflow from reservoirs, and reservoir operation patterns that are critical to understanding the human impact, are not derived. A similar and more regionalized system for monitoring reservoirs is the recent Mekong Dam Monitor created by the Stimson Center (<https://www.stimson.org/project/mekong-dam-monitor/>). While the breadth of information provided by Mekong Dam Monitor is extensive, to the best of our knowledge, the system is not open-source where all the source code and inputs are made publicly available to ensure reproducibility and scalability to other regions of the world.

In response to current limitations of the existing state of the art on reservoir monitoring systems, Biswas et al. (2021) introduced an open-source and reproducible tool based on satellite observations hydrological modeling-based called the Reservoir Assessment Tool (RAT; [https://depts.washington.edu/saswe/rat\\_beta/](https://depts.washington.edu/saswe/rat_beta/)). It is currently operational for a total of 1598 reservoirs around the world with scripts and data processing methodologies made fully public. Since it is the first version (1.0) of such a global and reproducible tool, we refer to it as RAT 1.0 in the rest of the manuscript. RAT 1.0 reports the daily modeled reservoir inflow, monthly surface area variation, storage change and outflow, and the inferred rule curve for South America, Africa, South and Southeast Asia. The open-source nature of the project encourages stakeholders to freely use the framework and add features needed by stakeholders. For example, RAT 1.0 framework has been successfully used to develop a RAT for simultaneous management of water quantity and water quality (RAT-WQ<sup>2</sup>) by several stakeholder agencies, such as by the Center for Water Resources Development and Management (CWRDM) of Kerala (India) (<http://depts.washington.edu/saswe/kerala/>), and for the Nile River Basin (NiBRAS; <https://depts.washington.edu/saswe/nibras/>; Eldardiry and Hossain, 2019; Eldardiry and

Hossain, 2021a).

In this paper, we propose the second version (2.0) of the RAT framework, with various improvements in accuracy and functionality, based on continuous feedback received from stakeholders of the Mekong basin. This second iteration of improvement of the RAT framework is hereafter referred to as RAT 2.0 in the manuscript. Our motivation for developing RAT 2.0 is driven by the need for continuous improvement based on the increasing availability of satellite remote sensing data from multiple sensors, hydrologic model improvements and innovations in information technology (IT). Another goal for the development of RAT 2.0 is the need to improve the accuracy of prediction of reservoir's dynamic state to a level that triggers more actionable decision making for stakeholder agencies such as the Member Countries of the Mekong River Commission (MRC), including Cambodia, Lao PDR, Thailand and Viet Nam. Continuous feedback was obtained via close deliberations with the MRC during a year-long period spanning March 2021–May 2022. These deliberations were based on the global version of RAT 1.0. Based on this year-long feedback from the MRC and the need for continuous improvement, the design goals of RAT 2.0 that drove the current study were as follows:

1. Improve the temporal resolution of the reservoir's dynamic state prediction from monthly, to weekly to sub-weekly allowing a more granular tracking of upstream reservoir operations.
2. Improve accuracy of reservoir storage change and outflow in RAT 2.0, by leveraging advanced water classification methods and a larger suite of satellite remote sensing data.
3. Provide outflow forecasting functionality in RAT 2.0 based on user-provided operating scenarios to allow stakeholders more lead time in responding to likely impacts of upstream dam operation.

The key research question we aim to address in this paper is – *how skillfully can a reservoir's dynamic state, specifically, the surface area change, storage change, and outflow, be predicted using a more comprehensive suite of satellite sensors, methodological advances, and an improved information technology framework?* Our hope with the continued improvement of the RAT from RAT 1.0 to RAT 2.0, is to empower stakeholder agencies with information on reservoir operations using publicly available satellite observations that can improve decision-making for water resources management, while honoring the goals of open-access, reproducibility, and scalability. The paper is organized as follows: Section 2 provides a short description of the study region of the Mekong River Basin over which where RAT 2.0 was developed and tested. Section 3 describes the data, models and methods used in RAT 2.0 that comprise key improvements to RAT 1.0. Section 4 discusses results, showcasing the overall skill of prediction of reservoirs' dynamic state. Finally, Section 5 summarizes the key finding, limitations, and recommendations for further work.

## 2. Study region: The Mekong River Basin

Situated in South East Asia, the Mekong River is one of Asia's longest transboundary river systems, with a length of 4763 km. It passes through a total of six countries – China, Myanmar, Thailand, Lao PDR, Cambodia and Viet Nam, draining about 810,000 km<sup>2</sup> (Mekong River Commission, 2021). The seasonal cycle of the basin is driven by a tropical monsoonal climatic system, with the basin receiving most of the precipitation during the period of May to October (Hossain et al., 2017).

The Mekong River has been subject to increasing flow regulation in the recent past by the construction of reservoirs, especially due to an increasing demand for food, energy, and water for sustaining the rapidly growing economies of the region. The effects of this increased regulation are also very apparent in its current flow conditions, characterized by reduced flow during wet seasons and higher flows during dry seasons (Mekong River Commission, 2019, 2021), and a decreased sediment load (Kondolf et al., 2018; Mekong River Commission, 2019). The

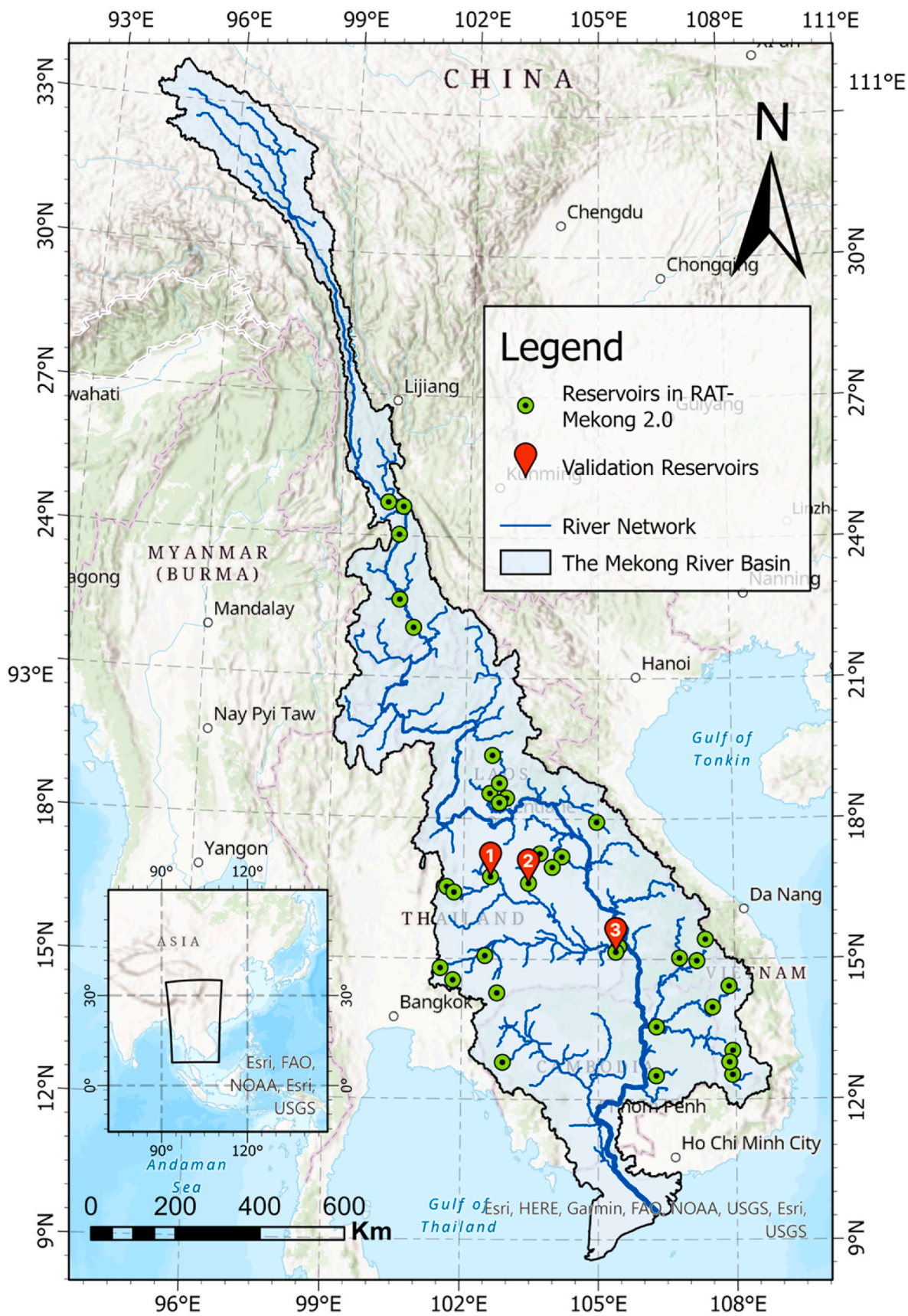


Fig. 1. Map of the study area, depicting the Mekong River and the reservoirs monitored in RAT 2.0. The validation reservoirs are as follows – 1: Lam Pao, 2: Ubol Ratana, 3: Sirindhorn.

**Table 1**  
Summary of satellite sensors used in RAT 2.0

Sensor	Spatial Resolution	Temporal Resolution (revisit period)	Sensor Type
Landsat-8 MSI (Surface Area)	30 m	16 Days	Optical
Sentinel-2 A/B MSI (Surface Area)	10–20 m	10 Days for a single satellite (~5 Days for two satellites)	Optical
Sentinel-1 C-band SAR (Surface Area)	10 m	10 Days	Synthetic Aperture Radar (SAR)
JASON-3 (Water Level)	~300 m	10 Days	Radar Altimetry

**Table 2**  
Summary of improvements introduced in RAT 2.0 as compared to RAT 1.0.

	RAT 1.0	RAT 2.0
Hydrological model rowhead	VIC 4.2.d (sequential computing)	MetSim + VIC 5 (parallel computing)
Evaporation rowhead	Obtained from VIC 4.2.d	Explicitly modeled using Penman Combination method
Satellite Sensors used to estimate Surface Area rowhead	Landsat 7, Landsat 8	Sentinel 1, Sentinel 2, Landsat 8 (TMS-OS algorithm), Jason-3 (Altimeter)
Surface Area, $\Delta S$ and Outflow temporal frequency rowhead	30 days	1–5 days
Area-Elevation Curve rowhead	SRTM derived	In-situ if available, otherwise SRTM derived
Outflow Forecasting rowhead	Not performed	Performed using GFS and historical/expected $\Delta S$

Mekong River Basin also houses the Tonle Sap Lake (TSL) system, which experiences one-of-its-kind hydrodynamic phenomenon of annual flow reversal due to the monsoonal flood pulse. In addition to providing significant economic, cultural and nutritional value to the inhabitants of the TSL region, it also supports a unique ecosystem and fisheries (Arias et al., 2012). Further dampening of the flood pulse due to upstream flow regulation can lead to cessation of the flow reversal phenomenon, leading to significant disruption to the ecosystem that it supports (Pokhrel et al., 2018).

The biodiversity supported by the Mekong River is currently categorized as relatively high (Dac Tran et al., 2020), with an estimated total of 924 species of fish, of which 219 are considered endemic to the basin (Valbo-Jorgensen et al., 2009). This biodiversity and the livelihood of a major portion of the population that depends on it are under direct threat by current and planned reservoirs (Ziv et al., 2012). These issues are not unique to the Mekong River Basin, as major river basins all over the developing world are facing similar problems due to increasing regulation through reservoirs. The Mekong River Basin may therefore be considered a microcosm of what is already happening or likely to happen to relatively undammed river basins of the developing world. Hence, lessons learned for the Mekong River Basin on reservoir operations monitoring using satellite data are expected to be relevant to other regions of the world. While the RAT 2.0 is developed using Mekong as an example, the usefulness and scalability of the new framework is therefore global.

The portion of the Mekong River's basin lying in the 4 downstream countries – Thailand, Lao PDR, Cambodia and Viet Nam – constitute the Lower Mekong Basin (LMB), while the upstream sub-basin in China and Myanmar is referred to as the Upper Mekong Basin (UMB). Established in 1995 by the LMB countries based on the principles of Integrated Water Resources Management (IWRM), the MRC is an intergovernmental organization that provides a platform for basin-wide dialogue and cooperation among the riparian countries of the Mekong River,

especially the LMB. Apart from providing an advocacy platform for the riparian countries, MRC also provides technical assistance and strategic advice to the member countries on sustainable development of the food, energy and water nexus. The MRC has been instrumental in providing feedback on the problems faced by downstream stakeholders and the solutions necessary for addressing them.

A total of 36 reservoirs of the Mekong River Basin are currently monitored in RAT 2.0. These reservoirs were initially selected from the Global Reservoir and Dam (GranD) database (Lehner et al., 2011). Three additional reservoirs were added for monitoring that were not in the GranD database based on the feedback obtained from the stakeholder agency. Location of all of the reservoirs is denoted in green in Fig. 1. Three Thai reservoirs out of these 36 reservoirs, Sirindhorn, Ubol Ratana and Lam Pao were selected for validation of the RAT 2.0 framework.

### 3. Data and methods

#### 3.1. Datasets

Publicly available data from a large array of currently operational remote sensing satellites, such as Landsat 8, Sentinel 1 and 2 make it possible to measure the reservoir surface area changes at a high temporal frequency. Highly accurate water level measurements at a 10-day temporal resolution can be made using Jason-3. RAT 2.0 improves both accuracy and temporal resolution of water area/level estimates using an ensemble of satellite sensors – Synthetic Aperture Radar (SAR) based Sentinel-1, Multispectral imaging-based Landsat-8 and Sentinel-2 A/B, and Radar altimetry-based JASON-3. A detailed discussion on the surface area estimation can be found in section 3.2.4. The reservoir surface area and water level elevation were estimated using an ensemble of sensors summarized in Table 1.

The in-situ area-elevation curve was also obtained from the Electricity Generating Authority of Thailand (EGAT, 2019). In-situ data on water fluxes – inflow, active storage, and outflow were obtained from the Royal Irrigation Department, Thailand (<http://app.rid.go.th:88/reservoir/>; RID, 2022). The data was obtained for three reservoirs in North-Eastern Thailand – Sirindhorn, Lam Pao and Ubol Ratana – for validation of the estimated fluxes.

Forecasted meteorological conditions were also obtained from the Global Forecasting System (GFS) (NCEP/NWS/NOAA/U.S. Department of Commerce, 2015) dataset to force the hydrological model to generate forecasted inflow in the reservoirs. The forecasted inflow was then used in conjunction with the inferred reservoir rule curve from Biswas et al. (2021) to estimate the forecasted outflow. A detailed discussion on the outflow forecasting component is provided in section 3.2.6.

#### 3.2. Methods

##### 3.2.1. RAT 2.0 model setup

The underlying core assumptions and design of the RAT 2.0 framework is similar to the original RAT 1.0 described in Biswas et al. (2021). The RAT framework comprises two main modules – (i) the hydrological modeling component, which provides the modeled inflow to reservoirs, and (ii) the satellite remote-sensing based reservoir observation component, which provides information on the changing reservoir state. The modular design of the framework allows RAT 2.0 to be model agnostic, and input data for any part of the components can be replaced easily with alternate options as necessary.

The dynamic state of the reservoir is modeled using the modeled fluxes to the reservoir and observed change in reservoir. At each reservoir, an assumption of conservation of mass is made –

$$O = I - E - \Delta S \quad (1)$$

where,  $O$  is the outflow from the reservoir,  $I$  is the inflow to the reservoir,  $E$  is the evaporation from the reservoir, and  $\Delta S$  is the storage

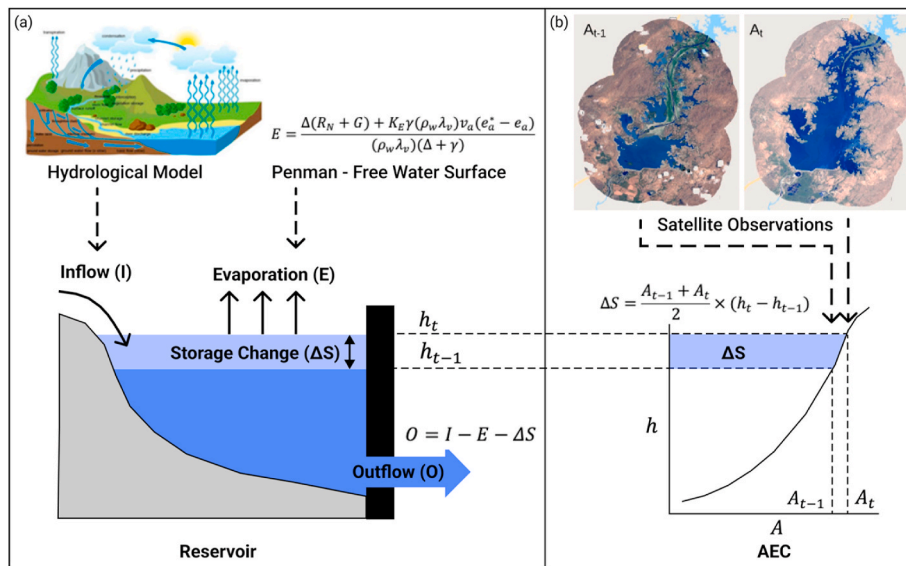


Fig. 2. (a) Conceptual model of the RAT 2.0 framework; (b) Illustration depicting the storage change estimation using satellite observations of surface area and the Area Elevation Curve (AEC).

change of the reservoir (Fig. 2 (a)). Ground seepage and precipitation on the reservoir are assumed to be negligible components of the reservoir mass balance. The Inflow is modeled using the Variable Infiltration Capacity – 5 (VIC 5) model (Hamman et al., 2018), but it can be swapped with any other hydrologic model. It must be noted here that the reported outflow from the reservoir in equation (1) is a combination of released water from the reservoir and all the other losses, such as lateral diversions, groundwater seepage losses and consumptive uses. Even though it would be much more meaningful for stakeholders to model the actual downstream releases from the dam via the spillway and penstocks, due to the current limitations of data sources, partitioning the outflow into its constituent fluxes such as lateral outflow, spilled flow and penstock flow, is not trivial. This limitation of a mass balance-based reservoir modeling schema has to be considered by stakeholders when using the outflow estimated by the RAT framework.

The storage change ( $\Delta S$ ) of the reservoir is estimated by assuming a trapezoidal bathymetry of the reservoir.

$$\Delta S = \frac{A_{t-1} + A_t}{2} \times (h_t - h_{t-1}) \quad (2)$$

Here,  $\Delta S$  refers to the total volumetric storage change,  $A_t$  and  $A_{t-1}$  refer to the observed surface areas from satellite remote sensing. The  $h_t$  and  $h_{t-1}$  are the water levels associated with the surface areas for time  $t$  and  $t - 1$  (Fig. 2 (b)). The  $h$  and  $A$  values, estimated from satellite data, are related to each other through the Area Elevation Curve (AEC) relationship. This allows for storage change estimations using either two successive satellite-based surface area observations, or two successive satellite altimeter-based water level elevation estimates.

The AEC relationship of each reservoir was calculated using the SRTM 1-Arc Second (30 m resolution) Global Digital Elevation Model (DEM) (Earth Resources Observation And Science Center, 2017). The SRTM DEM was generated using SAR technology, which is limited in its ability to penetrate water surfaces to obtain the bathymetric elevation information. This means that the directly observable bathymetry is limited to above the water elevation that existed during SRTM overpass. To address the issue of missing bathymetry below the water level, we generated the AEC by a combination of additional observations from other satellite sensors and extrapolation. The AEC generation methodology is further described in Biswas et al. (2021), which extrapolates the AEC below the water surface using a fitted power law curve. Given the modular nature of RAT 2.0, topographical survey-based AEC was also used when available to understand the impact of AEC quality on the

prediction of reservoir outflow.

### 3.2.2. Hydrological modeling: VIC-5 and MetSim

The RAT 2.0 framework is designed to be hydrological model agnostic, and hence users can use their preferred hydrologic model if needed. The current hydrological model used in RAT 2.0 during development is VIC 5 (Hamman et al., 2021). This model has a number of improvements compared to VIC 4.2.d (Hamman and Nijssen, 2016) which was used in RAT 1.0. A discussion on the improvements can be found in Hamman et al. (2018).

The meteorological simulation and forcing disaggregation are decoupled from the hydrological modeling routines in VIC 5, and are packaged as a separate model – MetSim model (Bennett et al., 2020). MetSim was used to perform the meteorological simulation at a 6-h timestep using (i) the daily minimum and maximum temperatures, (ii) daily precipitation, and (iii) wind speed, as inputs. These meteorological forcings are then disaggregated to – (i) average air temperature, (ii) total precipitation, (iii) pressure, (iv) incoming shortwave radiation, (v) incoming longwave radiation, (vi) vapor pressure, and (vii) wind speed.

Using the disaggregated forcings obtained from MetSim, VIC 5 was run at 0.0625° grid resolution for the Mekong River Basin. The model is run in parallel computing mode, exploiting the native support for the Message Passing Interface (MPI) standard, resulting in drastic improvements to performance. The VIC Routing model (Lohmann et al., 1998) was used to perform streamflow routing for the basin. Dominant River Tracing (DRT) based flow directions at 0.0625° spatial resolution by Wu et al. (2011) were used in the routing model.

In the current scheme of RAT 2.0, an explicit representation of inflow regulation by upstream reservoir was not performed. The inflow regulation was omitted in the current scheme for two reasons – (a) most of the reservoirs (21 out of 36) studied in this study are situated in separate tributaries of the Mekong river and lack upstream reservoirs; (b) even in the few cases (15 out of 36) when upstream reservoirs are present on the same stream, they are situated several hundreds of kilometers away. Due to these reasons, we believe inflow regulation by upstream reservoirs will have a negligible effect on the downstream reservoirs in the currently modeled reservoirs of the Mekong. The overall higher performance metrics for the three validation reservoirs of RAT 2.0 over RAT 1.0 also underscore that inflow regulation has a negligible effect in these reservoirs, and RAT 2.0 is still able to produce more accurate predictions. However, we recognize that to improve the global utility of

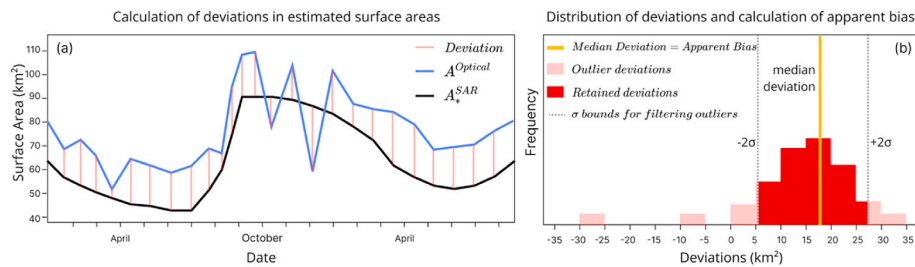


**Fig. 3.** Illustration depicting calculation of apparent bias using dummy data. (a) Depiction of calculation of deviation between  $A^{Optical}$  and  $A_s^{SAR}$ . The deviation between these time-series were used to estimate the apparent bias of  $A_s^{SAR}$ . (b) The distribution of the deviations between the two time-series (dummy data, for illustrative purposes). Since the reported surface areas can have unusually high deviations during challenging conditions (outliers) – seen at the tail ends of the distribution, a standard deviation threshold-based filtering was performed to discard these outliers. The median of the retained deviation values was then calculated, which was defined as the

apparent bias.

RAT 2.0, upstream regulation will have to be actively modeled, which we hope to carry out in a future iteration of improvement of the RAT framework.

### 3.2.3. Evaporation – penman equation

In contrast to RAT 1.0, where the modeled Evaporation from the VIC hydrological model was used, the evaporation in RAT 2.0 is modeled explicitly using the Penman Equation. Also known as the combination equation, the Penman equation for free water surface (Penman, 1948; Van Bavel, 1966) is defined as follows –

$$E = \frac{\Delta(R_N + G) + K_E \gamma (\rho_w \lambda_v) v_a (e_a^* - e_a)}{(\rho_w \lambda_v) (\Delta + \gamma)} \quad (3)$$

where,  $E$  is the evaporation;  $\Delta$  is the slope of the saturation vapor pressure – temperature relation;  $R_N$  is the net incoming radiation;  $G$  is the ground heat flux, which can be assumed to be 0 for daily calculations;  $K_E$  is the mass transfer coefficient, see (Dingman, 2015, p. 259; Harbeck, 1962),  $\gamma$  is the psychrometric constant;  $\rho_w$  is the water density;  $\lambda_v$  is the latent heat of vaporization;  $v_a$  is the wind speed;  $e_a^*$  and  $e_a$  are the saturation and actual vapor pressure for the air temperature. This volumetric evaporative loss [ $L^3 T^{-1}$ ] was estimated by multiplying the evaporation [ $L T^{-1}$ ] with the latest observed surface area of the reservoir.

### 3.2.4. High-frequency surface area estimation – A Tiered Multi-Sensor (TMS) approach

High temporal resolution of the storage change and outflow estimates is crucial for stakeholders to understand weekly to sub-weekly reservoir operations of upstream reservoirs. RAT 1.0 quantified the reservoir surface area at a monthly resolution by mosaicking Landsat scenes. The advantage of this approach is that mosaicking of multiple Landsat scenes helps address the effect of cloud cover that can cause a loss of accuracy in the reservoir surface area estimation. The disadvantage of this approach, however, is the inability to quantify any sub-monthly reservoir operations.

Hence, to address the need for modeling sub-monthly reservoir operations, a novel multi-sensor surface area estimation algorithm with a tiered self-correction process was developed. This method takes advantage of the strengths of both optical and SAR sensors in a team-work fashion. Optical sensors can very accurately estimate the water area (Cordeiro et al., 2021), but they can be highly limited by the presence of clouds. They also can be uncertain around dendritic reservoir shorelines if the perimeter is significantly larger than the nominal surface area (Biswas et al., 2021). On the other hand, SAR can penetrate clouds and is hence not affected by the presence of clouds. However, SAR backscatter threshold-based water extent estimation methods are highly sensitive to the choice of the chosen threshold, and have a tendency to underestimate the surface areas in inundated vegetation (Ahmad et al., 2020). This method combines the high accuracy of optical sensors with the cloud penetrating property of SAR sensors. This method is referred to as TMS-OS (Tiered Multi-Sensor approach – Optical, SAR,

pronounced as *Teams-OS*) in the rest of the manuscript.

The first module processes Sentinel-2 and Landsat-8 scenes in GEE to obtain the reservoir surface area using recommendations and findings from Cordeiro et al. (2021). The Region of Interest (ROI) was first delineated by taking a buffer around the reservoir boundary. The buffer distance was taken as 500 m by default, but is user configurable. The Sentinel-2 L2A – Surface Reflectance overlapping the ROI was scaled, and clouds were masked using the Scenes Classification Map (SCM) band in the preprocessing stage. Landsat-8 L2 Collection 2, Tier 1 – Surface Reflectance scenes overlapping the ROI were also identified, and clouds were masked using its pixel quality bitmask band (QA\_PIXEL). The scenes with more than 90% cloud cover over the ROI were filtered out due to extreme cloud cover conditions, and no further processing was performed.

The cascade simple k-means clustering algorithm (Google, 2022) was used to perform unsupervised classification on a subset of pixels sampled from cloud-masked scenes. The best value for k was chosen based on the Calinski and Harabasz (1974) criterion. The cluster with the highest Multiband Water Index (MBWI) (Wang et al., 2018) was then classified as the cluster of water pixels. This cascade k-means model was then used to classify the entire scene into water and non-water pixels. The Normalized Difference Water Index (NDWI) and B12 (2.185 – 2.202  $\mu\text{m}$ ) bands were selected for Sentinel-2, and the NDWI, Modified Normalized Difference Water Index (MNDWI) and B7 (2.107 – 2.294  $\mu\text{m}$ ) bands were selected for Landsat-8 as features for training the clustering model. These features were chosen after assessing the relative performance of a combination of various features (Cordeiro et al., 2021).

After classifying the unmasked pixels as water or non-water, the Zhao and Gao (2018) method of classifying masked pixels as water/non-water based on historical water probability (Pekel et al., 2016) was employed. The water classification and cloud mask correction components were both implemented in GEE, resulting in minimal on-premise computing requirements. The resulting reservoir water area time-series of 16 and 5-day temporal resolutions from Landsat-8 and Sentinel-2, respectively, were combined to obtain a time-series of 1–5-day frequency ( $A^{Optical}$ ).

Even after employing skillful unsupervised clustering method for classifying water and correcting for cloud-cover related artifacts, the time-series can still have unrealistic drop or gain in surface area estimates. This can happen for several reasons, especially owing to complete automation of the processing pipeline – such as sub-optimal choice of K by the Calinski and Harabasz (1974) criterion, or inability of the Zhao and Gao (2018) algorithm to completely filter out cloud related artifacts. Since SAR can penetrate clouds, a reasonable assumption was made that Sentinel-1 will be able to accurately quantify the trends of reservoir surface area correctly as increasing or decreasing even if there is quantitative mis-match from ground observations. Hence, further filtering and a novel trend-based correction using Sentinel-1 (SAR) was applied to the optically derived surface area time-series.

In the first tier of filtering, the areas reported by optical sensors are compared against Sentinel-1 after applying a bias-correction step. The

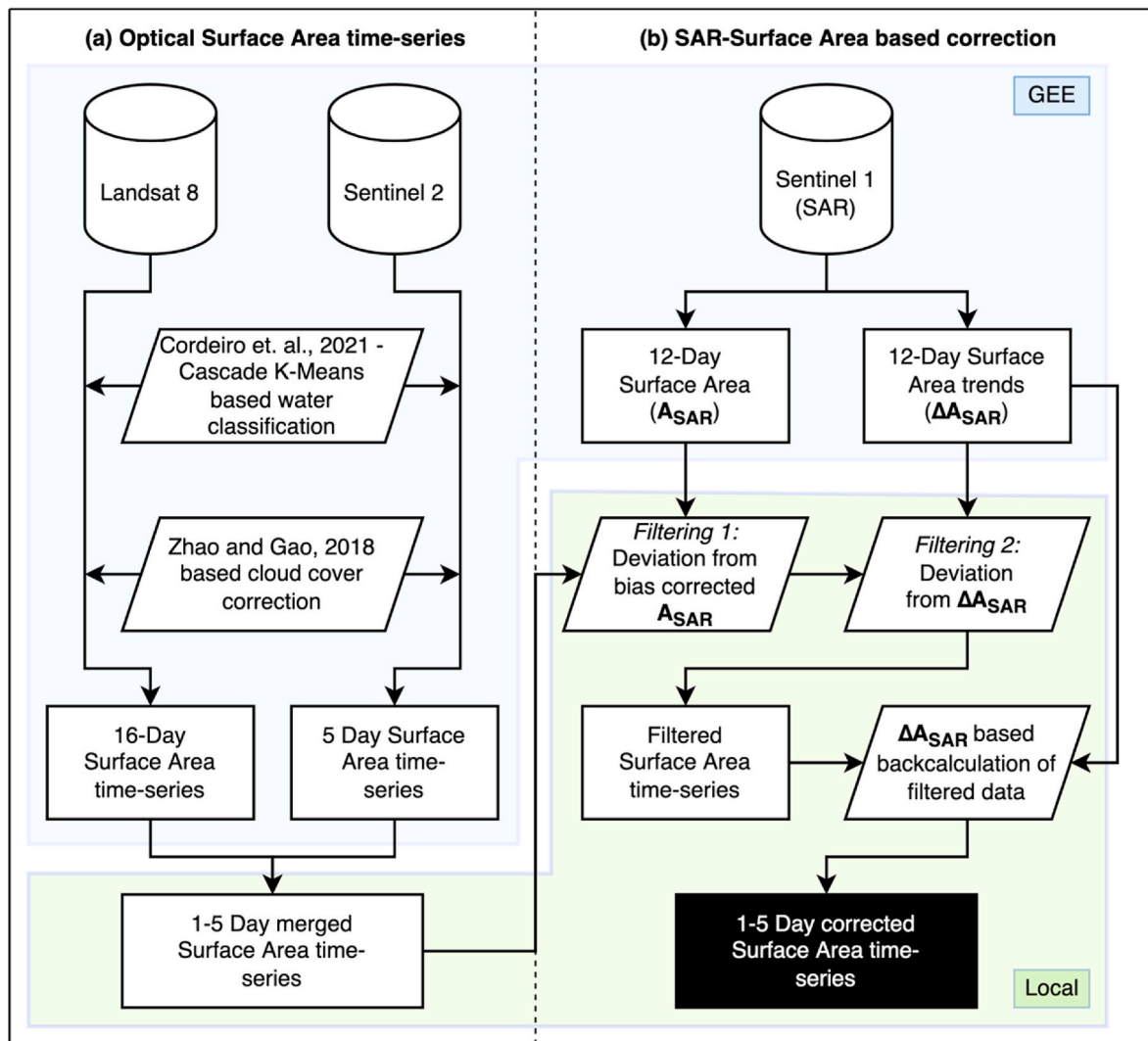


Fig. 4. Flow chart describing the TMS-OS algorithm. (a) Reservoir surface area estimation using unsupervised clustering (Cordeiro et al., 2021) and cloud-cover correction (Zhao and Gao, 2018); (b) SAR trend based filtering and correction of reservoir surface area time series. The blue and green shaded regions indicate if the processing is done in the GEE cloud or locally, respectively.

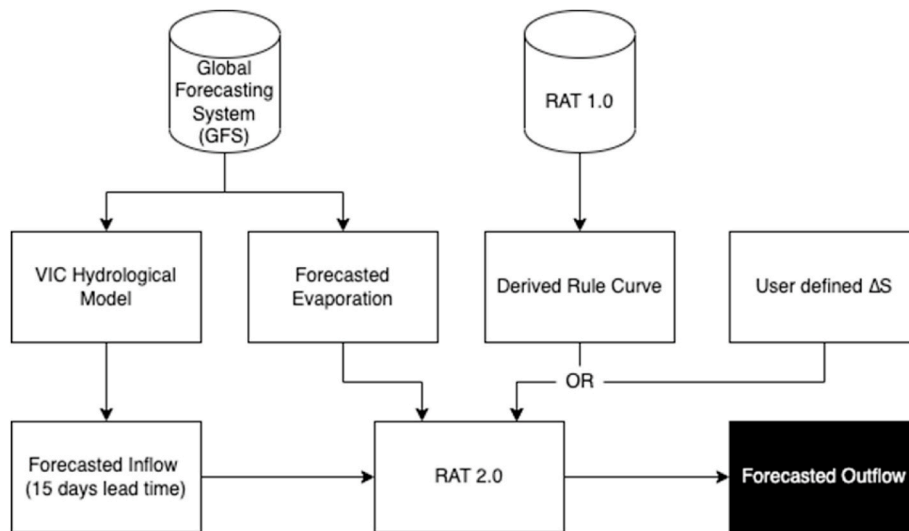
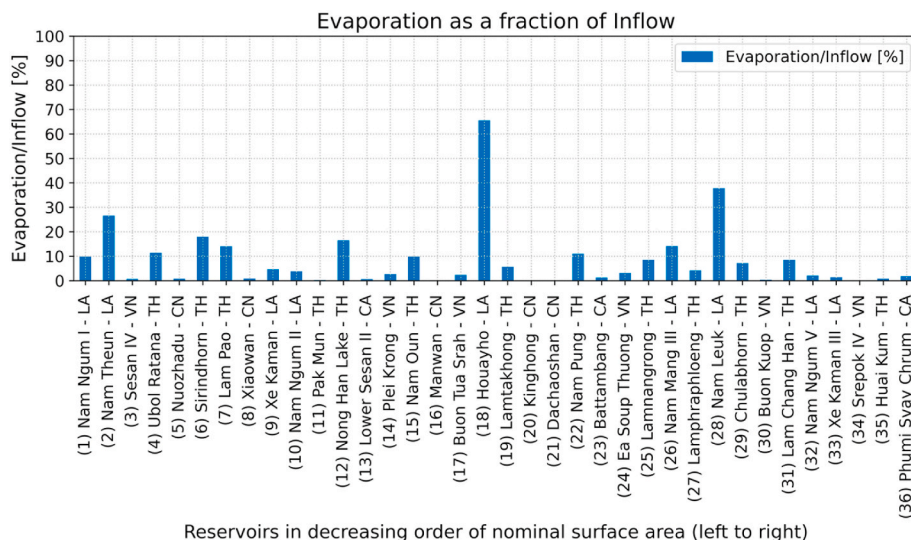
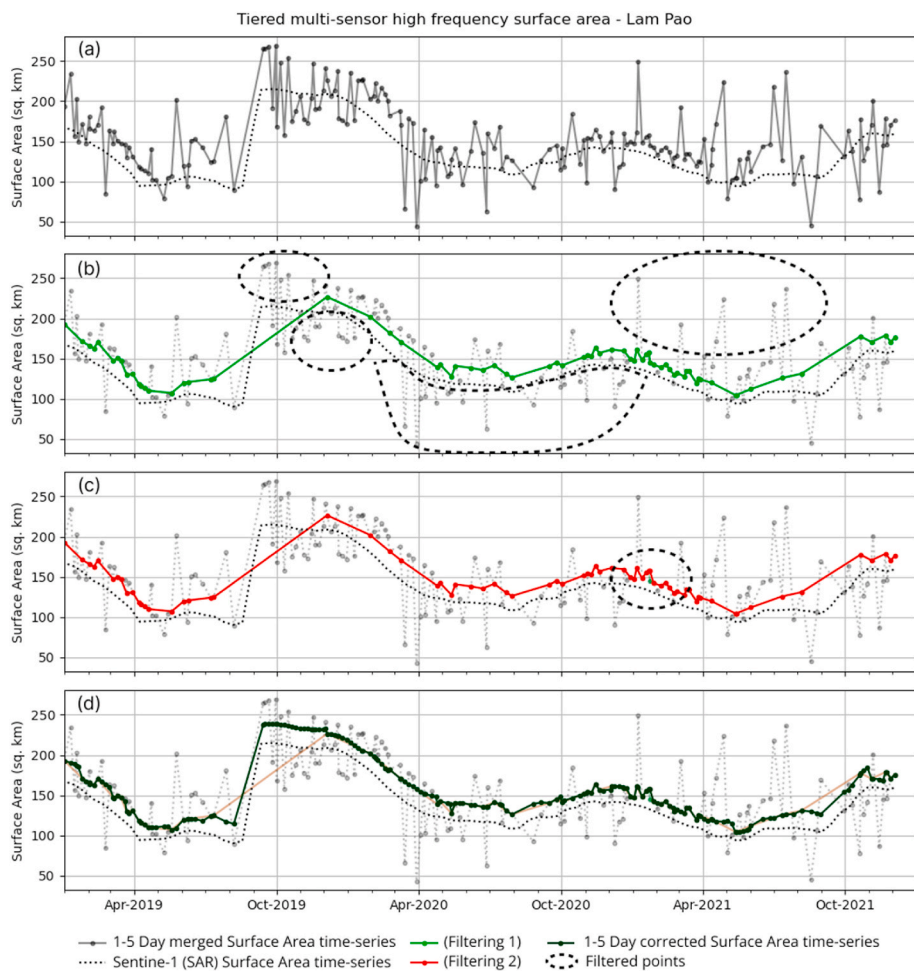


Fig. 5. Flowchart illustrating outflow forecasting functionality of RAT 2.0.



**Fig. 6.** Average monthly evaporative losses compared to average monthly inflow at selected reservoirs in the Mekong River Basin. The suffixes denote the country where the reservoirs are located – CA: Cambodia, CN: China, LA: Lao PDR, TH: Thailand, and VN: Viet Nam.



**Fig. 7.** Illustration of progressive tiers of filtering and correction in TMS-OS for the Lam Pao reservoir, Thailand. (a) 1–5 Day optically derived reservoir surface area time-series using clustering based classification and Zhao and Gao (2018) cloud-correction. (b) Filtering 1: Filtering based on deviation from bias corrected SAR surface areas. (c) Filtering 2: Filtering based on deviation from SAR surface area trends. (d) 1–5 Day corrected surface area time-series obtained by back-calculation of filtered data points using SAR surface area trends.

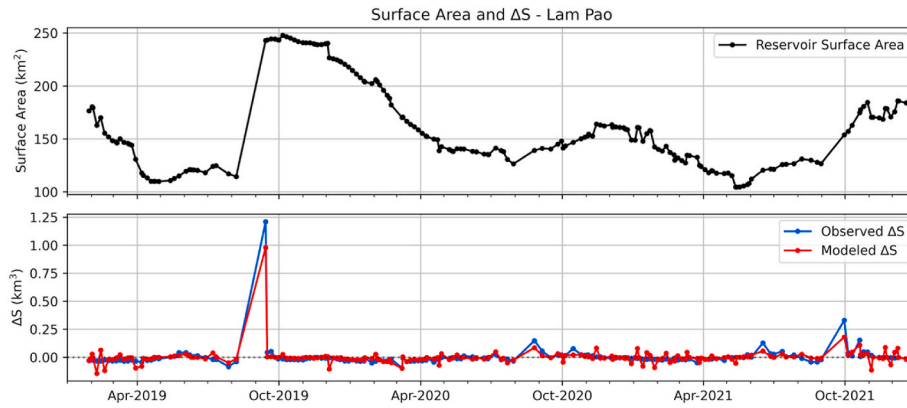


Fig. 8. Comparison of modeled storage change using surface area observations obtained using the TMS-OS methodology with observed storage change for Lam Pao, Thailand.

Table 3

Statistics comparing storage change modeled by RAT 2.0-TMS-OS (1–5 days), RAT 2.0-Altimeter (10 days), and RAT 1.0 (monthly) with observed storage change for the time period 2019–2021. Acronyms of performance metrics used - KGE: Kling-Gupta Efficiency (Gupta et al., 2009); RMSE: Root Mean Squared Error; MAE: Mean Absolute Error.

	Metric	RAT 2.0 (TMS-OS)	RAT 2.0 (Altimetry)	RAT 1.0
<b>Sirindhorn</b>	Correlation	0.61	0.85	0.33
	KGE	0.41	0.68	-2.4
	Normalized RMSE	8.3%	6.5%	15.8%
	Normalized MAE	5.1%	5.0%	9.7%
<b>Lam Pao</b>	Correlation	0.91	0.80	0.71
	KGE	0.58	-0.03	-0.63
	Normalized RMSE	3.4%	8.2%	13.8%
	Normalized MAE	2.1%	5.6%	8.6%
<b>Ubol Ratana</b>	Correlation	0.78	-	0.74
	KGE	-0.27	-	0.12
	Normalized RMSE	9.8%	-	16.4%
	Normalized MAE	4.9%	-	10.6%

reservoir surface area time-series ( $A^{SAR}$ ) was first obtained by applying backscatter thresholding method described in Ahmad et al. (2020) on Sentinel-1 SAR GRD: C-band data in GEE. The  $A^{SAR}$  was linearly interpolated to the frequency of  $A^{Optical}$ , referred to as  $A_z^{SAR}$  in the manuscript.

The deviations between the time-series were defined as the difference in reported areas by both the sensors -  $deviations = A^{Optical} - A_z^{SAR}$ , obtaining a distribution of the deviations. The apparent bias between both the time-series can be obtained by taking the median of the distribution of deviations, if there were no outliers. However, since the  $A^{Optical}$  time-series can contain outlier values due to challenging scenarios as described above which can skew the estimated median, a further filtering step was performed using a standard deviation ( $\sigma$ ) threshold. Using a trial-and-error method, a threshold value of  $\pm 2\sigma$  was found to be skillful in filtering out these outliers, by discarding deviation values outside the  $\pm 2\sigma$  range. Finally, the apparent bias (*bias*) was calculated as the median deviation of this filtered distribution. This filtration step and calculation of *bias* is illustrated pictorially in Fig. 3 using dummy data.

The normalized deviations were then calculated as:  $norm. deviations = deviations - bias$ . Data points were filtered if the normalized deviation was greater than a defined threshold value. Using a trial-and-error method, a threshold value of  $\sim 5\%$  of the nominal surface area of the reservoir was found to be skillful at filtering out physically unrealistic surface areas.

The normalized deviations were then calculated as:  $norm. deviations = deviations - bias$ . Data points were filtered if the normalized deviation was greater than a defined threshold value. Using a trial-and-error method, a threshold value of  $\sim 5\%$  of the nominal surface area of the reservoir was found to be skillful at filtering out physically unrealistic surface areas.

A second tier of filtering was applied to the dataset by comparing the reservoir water area change trends estimated by optical and SAR sensors. Data points were filtered out if the difference in trends was greater

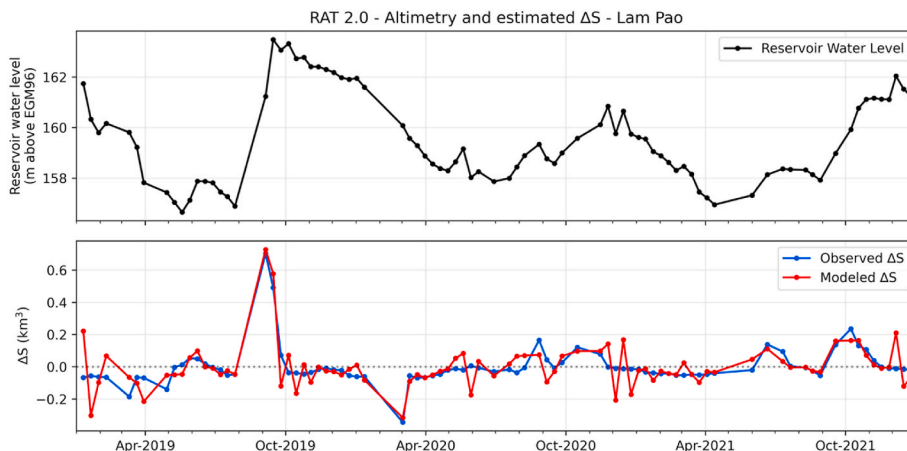


Fig. 9. Comparison of modeled storage change using altimeter measurements of reservoir water level with observed storage change for Lam Pao, Thailand.

**Table 4**

Statistics comparing outflow modeled by RAT 2.0-TMS-OS (1–5 days), RAT 2.0-Altimeter (10 days), and RAT 1.0 (monthly) with observed outflow for the time period 2019–2021. Acronyms of performance metrics used - KGE: Kling-Gupta Efficiency (Gupta et al., 2009); RMSE: Root Mean Squared Error; MAE: Mean Absolute Error.

	Metric	RAT 2.0 (TMS-OS)	RAT 2.0 (Altimetry)	RAT 1.0
<b>Sirindhorn</b>	Correlation	0.55	0.47	0.11(p-val > 0.05)
	KGE	-0.08	-0.02	-0.51
	Normalized RMSE	11.3%	23.8%	28.6%
	Normalized MAE	6.0%	17.6%	19.4%
	<b>Lam Pao</b>	Correlation	0.38	0.27
	KGE	-0.3	-0.29	-0.63
	Normalized RMSE	8.1%	16.4%	45.9%
	Normalized MAE	2.7%	9.5%	33.7%
<b>Ubol Ratana</b>	Correlation	0.13(p-val > 0.05)	-	-0.07(p-val > 0.05)
	KGE	-0.3	-	-0.72
	Normalized RMSE	10.5%	-	34.4%
	Normalized MAE	4.4%	-	24.2%

than a defined threshold value. Using a trial-and-error method, a threshold value of ~5% of the nominal surface area of the reservoir was found to work well as the threshold value in weeding out unrealistic drops in  $A^{Optical}$ . The trend is defined as follows:

$$trend^{SAR} = \frac{A_{*}^{SAR}(t_2) - A_{*}^{SAR}(t_1)}{t_2 - t_1} \quad (4)$$

where,  $t_1$  and  $t_2$  are dates of observation of optical sensors (1–5-day resolution) and  $A_{*}^{SAR}(t_1)$  and  $A_{*}^{SAR}(t_2)$  are the interpolated areas on the respective dates by the SAR Sentinel-1 sensor. Similarly, the trends in  $A^{Optical}$  were also obtained.

Finally, a trend-based correction step was applied to fill in the filtered data points using the apparent trend in surface area change estimated by the SAR sensor,  $trend^{SAR}$ . This step assumes that, even if  $A^{SAR}$  are biased, the bias term will get cancelled out while calculating  $trend^{SAR}$ . For each point that was filtered out in the tiered filtering steps, the data was filled by estimating the area using  $trend^{SAR}$  as follows –

$$A'_{(t_2)} = A_{(t_1)} + (trend^{SAR} \times (t_2 - t_1)) \quad (5)$$

where,  $t_2$  is the date of observation of a data point that was filtered out, and  $t_1$  is the previous date of observation.  $A'_{(t_2)}$  is the area estimated by the trend correction step, and  $A_{(t_2)}$  is the area observed on  $t_1$ . This calculation was performed iteratively for all the filtered data points to obtain the final 1–5 day trend-corrected reservoir surface area time-series. The TMS-OS algorithm is summarized in Fig. 4

This 1–5 day frequency reservoir surface area time-series obtained using TMS-OS was then used to obtain the storage change using equation (2). Using this storage change estimate, along with the inflow from the hydrological model and the evaporation using the penman equation, the outflow was estimated using equation (1).

### 3.2.5. Water level – altimetry

The reservoir water level was also mapped using the Jason-3 radar altimeter, in addition to estimating the reservoir surface area using optical and SAR sensors. Radar altimetry-based water level estimates are highly accurate, however, their applicability in regional to global reservoir mapping is limited due to poor spatial coverage and temporal

resolution of the sensors. Due to the sparse spatial coverage of the Jason-3 altimeter, we validated the use of altimeter data over two reservoirs as a proof of concept to show how RAT 2.0 can benefit from altimeter-type data on reservoir elevation when available.

The water level ( $h$ ) of reservoirs were estimated using the Okeowo et al. (2017), an automated clustering based method for obtaining in-land water surface elevations from Jason-3 observations. Although the Okeowo et al. (2017) method is quite robust for most cases as it uses a k-means clustering technique, there will always be challenging cases that warrant a final statistical sanity check and adjustment. For example, when the altimeter ground track has a short length over the reservoir or is near the shoreline, the reported height may be erroneous, especially if the reservoir shoreline contracts substantially due to reservoir draw-down or during a drought. These outliers appear as sudden jumps in the estimated reservoir water level, and were filtered using a standard deviation threshold-based method.

For an observation, the standard deviation was calculated in a rolling window of 4 preceding (left standard deviation -  $\sigma_l$ ) and 4 following (right standard deviation -  $\sigma_r$ ) observations. A filtration condition was then defined, such that, if both the left and right standard deviations were higher than 2 standard deviations, then the data points were filtered out. The threshold value of 2 standard deviations was chosen based on a trial-and-error basis such that most of the outliers were filtered out, and the authors recommend selecting a threshold value specific to each reservoir based on the intersection of the ground track with the reservoir. The rationale of the filtration step is as follows – if a data point is more than 2 standard deviations as compared to both previous and next observations, then it is very likely that the data point does not reflect an actual rise or decrease in the water level, and hence can be filtered out, and *vice versa*. The filtered out points were then filled by linearly interpolating the neighboring observations. The AEC was then used to obtain the corresponding surface area of the reservoir and the storage change was then estimated using equation (2).

### 3.2.6. Outflow forecasting

In addition to providing nowcast and historical (hindcast) estimates of outflow, the functionality to forecast outflow for a 15-day lead time was also added to RAT 2.0. The forecasted meteorological conditions – minimum and maximum temperature, u- and v-components of wind speed, and precipitation – obtained from the GFS dataset were used to force the VIC hydrological model to estimate the forecasted inflow to the reservoirs. The forecasted evaporation was also estimated using equation (3) with forecasted meteorological conditions obtained from the GFS dataset.

The RAT 2.0 forecasting framework provides two options of rule-curve based estimation of outflow for a 15-day lead time – (1) satellite derived rule curve from RAT 1.0, (2) user defined rule curve or time-varying target storage (see Fig. 5). The rule curve in RAT 1.0 is derived based on averaging the historical storage change patterns over a multi-year period for each month, and then inferring the most likely storage target ( $S$ ) that the reservoir has tried to achieve, as a fraction of the maximum storage ( $S_{max}$ ). The rule curves are then interpolated to a 5-day frequency using linear interpolation. The interpolation is performed to stay consistent with the pentad frequency of hindcasted  $\Delta S$  using the TMS-OS approach. The expected storage change is then estimated from the interpolated derived rule curve as follows –

$$\Delta S_T = (S_0 / S_{max} - S_T / S_{max}) \times S_{max} \quad (6)$$

where  $\Delta S_T$  is the expected storage change as a percentage of maximum storage based on rule curve for lead time,  $T$ .  $S_T / S_{max}$  corresponds to the storage as a fraction of maximum storage at lead time  $T$ , and  $S_0 / S_{max}$  corresponds to the storage as a fraction of  $S_{max}$  for the current time-step. The  $S_T$  can be obtained either from the inferred rule curve (option 1) or from a user-defined target storage at  $T$ . The  $S_{max}$  can be obtained either from in-situ data, or from dam metadata repositories, such as the GRand

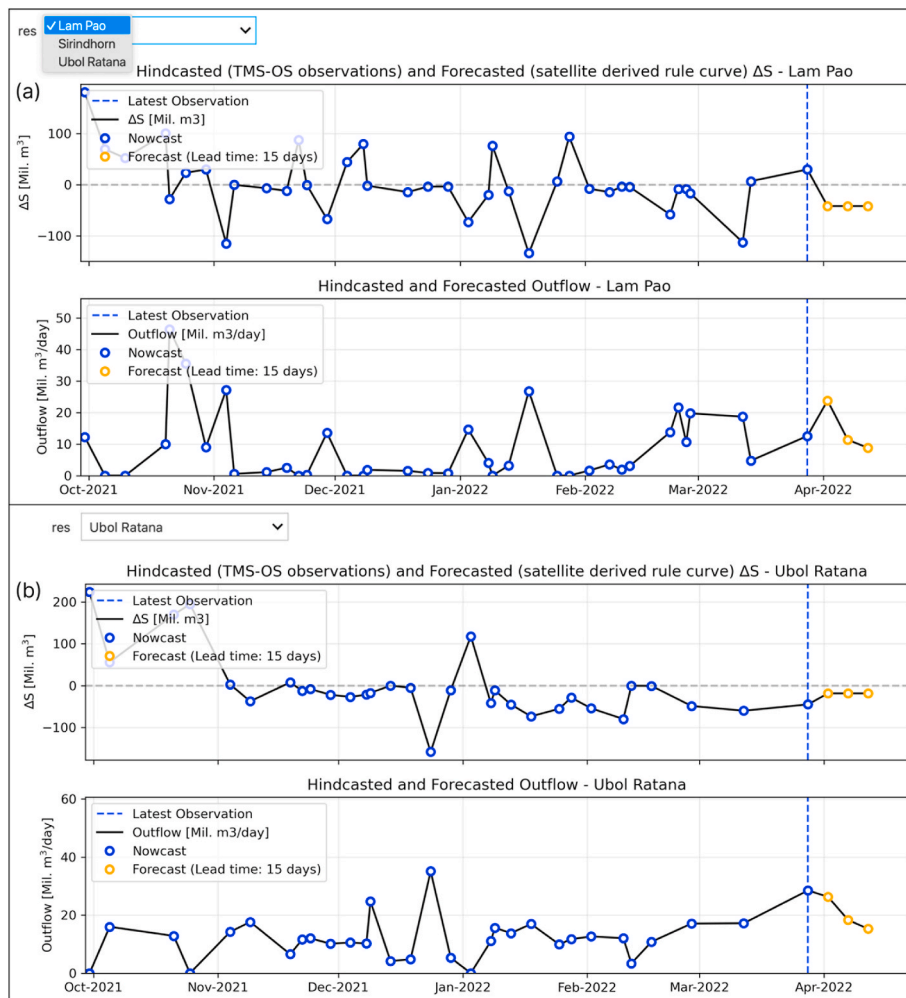


**Fig. 10.** Forecasted outflow using historical satellite observations derived rule curve. (a) Conceptually, the reservoir of interest can be selected using the drop-down menu, with Lam Pao reservoir selected for visualization in the current case. (b) Selecting Ubol Ratana from the drop-down list updates the graphic to reflect forecasted outflow for the reservoir.

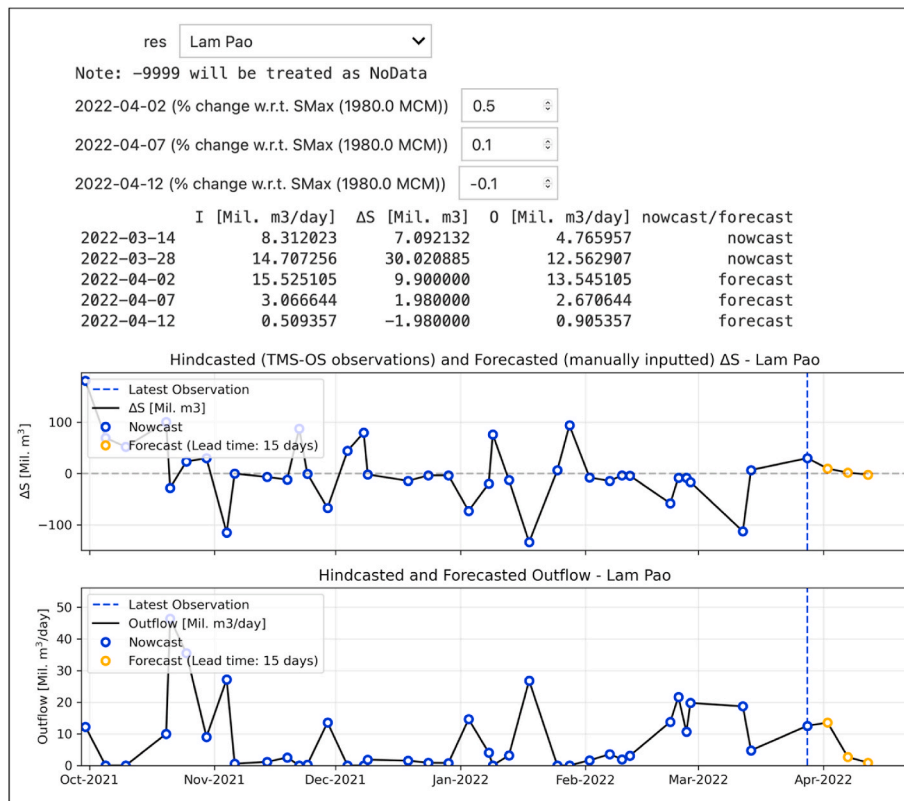


Fig. 11. Forecasted outflow using user-defined ΔS, as a percentage of maximum Storage of the reservoir.

database (Lehner et al., 2011). This expected storage change was used in the mass balance equation (1) to estimate the forecasted outflow.

$$O_T = I_T - \Delta S_T \tag{7a}$$

where  $O_T$ ,  $I_T$  and  $\Delta S_T$  are the outflow, inflow and storage change at a future time  $T$ . The evaporation was ignored due to the low contribution of the evaporation in dictating the outflow for the Mekong region. A discussion on the importance of evaporation for the Mekong basin is provided in section 4.1.

Since reservoir operations can highly depend on the on-site decisions made by the dam operator, antecedent conditions, and the need to meet storage and distribution targets, RAT 2.0 also provides the functionality to directly input the expected storage change for a given lead time and visualize the expected outflow for the same lead time.

### 3.2.7. Computational Configuration of RAT 2.0

The RAT 2.0 was developed and tested in a CentOS 7 Linux environment, setup on a high-performance server. The server is configured with  $2 \times 8$  core Intel Xeon Gold processors, each having 2 threads per code, equating to a total of 32 computing units. MetSim and the VIC hydrological model were both configured to make use of the 32 computing units for parallel computation. The main memory of the system totals to 192 GB, allowing for a high ceiling of in-core processing.

A data-processing module for pre-processing raw satellite data-products and transforming them into model inputs was developed. This module makes use of the high memory ceiling for performing data transformations as in-core operations to significantly improve the performance. While this implementation has high memory requirements,

the implementation can be easily changed to an out-of-core processing schema according to constraints.

In its current implementation, the RAT-Mekong model takes about 3 h to run for the Mekong basin. Due to high computational requirements, MetSim is run only for the newly acquired data with a spin-up time of 3 months. The VIC model is then run for the entire time period of 2000-current at a daily time-step to obtain basin-wide modeled runoff and baseflow. The VIC routing model is then used to route the modeled runoff and baseflow to obtain daily modeled streamflow (inflow) at the reservoirs. For generation of the modeled streamflow by the routing model, the station locations have to be defined as the coordinates in terms of indices of the grid array. A python script was created to perform the conversion from latitude-longitude values of stations to their respective array-index representation in the model grid.

The remote sensing module offloads the processing to Google Earth Engine’s (GEE) cloud computing infrastructure, and hence has minimal local processing requirements.

Currently, the RAT model is set up to run daily at a 3-day lag, to offset any data provider side delays and their inherent latency. For example, many satellite datasets have a 1–2 day latency, sometimes even longer with data outages. If there were no delays or latency associated with input data, then RAT 2.0 can theoretically produce outputs within 24 h of the most recent satellite observation. We anticipate such a scenario to be a reality as IT capabilities improve and latency decreases for satellite missions and data providers.

Compared to RAT 1.0, the web interface of RAT 2.0 is virtually unchanged, with only a new tab to show altimetry data for reservoirs that have JASON-3 overpasses. The new backend is available as an open-source project under the GNU General Public License v3.0 (GNU

GPLv3) license on GitHub at - [https://github.com/pritam47/rat\\_v2](https://github.com/pritam47/rat_v2).

The improvements in RAT 2.0 over RAT 1.0 are summarized in Table 2.

## 4. Results and discussion results

### 4.1. Reservoir evaporation

The evaporative losses were found to be very nominal for the South East Asian reservoirs, with flux magnitudes less than 10% of inflow for 30 out of 36 assessed reservoirs. The catchment areas of the remaining 6 reservoirs are relatively small, which generate low inflow volumes. Moreover, out of 6 other reservoirs, 5 are primarily used for hydroelectricity. Operators usually keep the reservoir close to full to maximize hydroelectricity production, which explains the higher evaporation compared to the natural inflow (see Fig. 6).

In general, the evaporation does not seem to be a major control on the water balance of the reservoirs of South East Asian River basins, which is consistent with previous study of [Bonnama et al. \(2016\)](#). However, in other river systems across the globe, evaporative losses may be significant for relatively drier river systems, such as in the Nile ([Eldardiry and Hossain, 2019](#)) and the Tigris-Euphrates. Since the RAT 2.0 framework is designed for global applications, the evaporative losses are still taken into account for the hindcast and nowcast of the outflow from reservoirs, even though the evaporative losses do not play a major role in the currently studied Mekong Region.

### 4.2. High-frequency surface area estimation – TMS-OS

The surface areas using TMS-OS were obtained for the period of 2019–2021 (3 years) due to the overlap of data between all the datasets – Sentinel-2, Landsat-8 and Sentinel-1. Fig. 7 (a) shows the 1–5 day surface area time-series obtained using the optical sensors employing the methodology described in Fig. 4 (a). At this step, rapid drops and rises in the estimated surface areas can be noted. These drops in surface areas do not reflect actual changes in reservoir surface area, rather, they are artifacts of the Cascade k-means clustering algorithm and limitations of the optical sensor to discriminate water from land. Since the [Calinski and Harabasz \(1974\)](#) criterion is used to select the number of clusters, a sub-optimal value for  $k$  can be selected by the criterion in case of challenging scenes. Such challenging scenes include, but are not limited to, cloud pixels that do not get identified accurately by the cloud masking algorithms, presence of high sediment load or algal conditions, or issues such as shadows in the scene due to terrain or clouds. In such cases, the clustering algorithm can select a higher value of  $k$ , that, even though has the lowest Calinski-Harabasz index value, the chosen cluster of water pixels may not represent all the water pixels in the scene. Choosing a sub-optimal value of  $k$  is a disadvantage of automatic selection of the number of clusters. However, these errors get identified, filtered and corrected in the next steps of the algorithm.

Fig. 7 (b) and (c) illustrate the surface area time-series after applying filtering-1 and filtering-2, respectively (see Fig. 4 for filtering methodology). At this stage, the filtered-out data points were replaced by no-data values. The number of points that get filtered out in each step highly depends on the choice of the threshold values. Using a trial-and-error method, a threshold value of ~5% of the nominal surface area of the reservoir for both the filtering steps was found to be a good balance between filtering out unphysical data points while retaining surface area values that could not be confidently identified as erroneous. These steps combined provide an automatic way of filtering out data points based on

the agreement between surface area estimates from two different sensors with complementary strengths.

Finally, Fig. 7 (d) shows the 1–5 day corrected surface area time-series, obtained by filling the previously filtered data points using trends from SAR derived surface area time-series. The resulting time-series is free of unphysical changes in reservoir surface areas. The accuracy of the estimated surface areas was tested by comparing the modeled storage change ( $\Delta S_{RAT}$ ) with observed storage change ( $\Delta S_{Obs}$ ) in section 4.3 (see Fig. 8).

### 4.3. Storage change

The modeled storage changes derived from RAT 2.0-TMS-OS, RAT 2.0-Altimetry and RAT 1.0 were compared against in-situ observed storage change. The in-situ storage change was defined as follows –

$$\Delta S_{Obs} = S_{(t2)} - S_{(t1)} \quad (7a)$$

where  $t1$  and  $t2$  are dates of consecutive satellite observation, and,  $S_{(t1)}$  and  $S_{(t2)}$  are the corresponding in-situ storages. The  $\Delta S$ , hence has a unit of  $[L^3]$ , representing the amount of storage change between consecutive satellite observations. The comparison metrics are summarized in Table 2.

The estimated storage change values using Jason 3 altimeter elevation data that were further corrected based on methodology described in section 3.2.5, were compared against the observed in-situ storage change. The comparison metrics are summarized in Table 3. Fig. 9 shows the derived water level after filtering out outliers, and the estimated storage change values overlaid on the observed in-situ storage change. With the highest correlation, the altimeter-based technique was found to be the most skillful in modeling the storage change, albeit at a 10-day frequency.

Since the comparisons were performed at the temporal resolution of the respective models, the statistics corresponding to RAT 2.0-TMS-OS quantify the performance at a 1–5 day frequency, RAT 2.0-Altimetry at a 10 day frequency, and RAT 1.0 at a 30 day frequency. This underlines the inherent improvement brought forth by RAT 2.0, that is, observing the reservoir dynamics at a pentad frequency or less using optical and SAR, and at 10-days using altimetry, as opposed to the monthly frequency of RAT 1.0. Even at this frequency, RAT 2.0 performs better for every metric. Overall, the Kling-Gupta Efficiency (KGE) ([Gupta et al., 2009](#)) of the RAT 2.0 represent an improvement over the RAT 1.0 estimates in most of the cases. For the TMS-OS based estimations, the average correlation increased from 0.59 to 0.77, the average normalized RMSE decreased from 15.3% to 7.1%, and the average normalized MAE decreased from 9.6% to 4.0%. The RAT 2.0-Altimetry based estimates perform the best, with an average correlation of 0.82, normalized RMSE of 7.3%, and a normalized MAE of 5.3%. However, the sparse spatial coverage of the altimetry method limits the number of mappable reservoirs.

### 4.4. 4.4.outflow

The outflow estimates obtained using equation (1) were compared with the observed outflows for the three validation reservoirs. Additionally, the outflow estimated by RAT 2.0 using the TMS-OS approach was compared against the outflows estimated by RAT 1.0 which are summarized in Table 4. The metrics were obtained for 1–5 day temporal resolution for RAT 2.0, and at a monthly frequency for RAT 1.0. Even at this higher temporal frequency, RAT 2.0 is able to improve the flux

estimations as compared to RAT 1.0.

Since the outflow is estimated by assuming water mass balance at the reservoirs, the errors in the constituent fluxes can add up, propagating forward into the estimated outflow. For this reason, even though RAT 1.0 was able to quantify the constituent fluxes, *i.e.*, inflow and storage change with reasonable accuracy, the estimated outflow deviated significantly from the observed outflow. However, the improvements in the accuracy of modeled constituent fluxes by RAT 2.0 using a multi-sensor and approach for improving data quality, now allows for quantifiably better outflow estimation. The KGE values for RAT 2.0 are higher as compared to RAT 1.0 across the board (Table 4). All the KGE values for RAT 2.0 are also better than  $-0.41$ , which is equivalent to the model performing as good as using the mean value of observations as a predictor (Knoben et al., 2019). The correlation of estimated outflow with the observed outflow at two out of three tested reservoirs increased from statistically insignificant correlation in RAT 1.0 to 0.38 and 0.59 for Lam Pao and Sirindhorn respectively. The normalized RMSE decreased from an average of 36.3%, to 10.6%, while the normalized MAE decreased from an average of 25.8%, to 4.6%.

#### 4.5. Outflow forecasting

Fig. 10 (a) shows the idea behind the outflow forecasting of RAT 2.0 for the Lam Pao reservoir. To demonstrate the functionality of the outflow forecasting module, an example date of 28<sup>th</sup> March 2022 was chosen as the “current” observation. The forecasted  $\Delta S$  was then derived using the rule curve for Lam Pao for a 15-day lead time at a 5-day temporal resolution to mimic the observations that can be obtained in that time-period. Using the simulated  $\Delta S$ , in conjunction with the forecasted inflow for the time-period, the forecasted outflow was visualized. The “res” drop-down can be used to choose the reservoir of interest. In the front-end of RAT 2.0, the user has the option to select the reservoir of their choice using the “res” drop down menu, as demonstrated in Fig. 10 (a). The three validation reservoirs were used for demonstration purposes for this manuscript.

Additionally, the second method of outflow forecasting, using  $\Delta S$  defined by the stakeholders, is presented in Fig. 11. The user has to first select the reservoir of interest using the “res” drop-down menu. Once chosen, the user is presented with a table showing the “nowcast” estimates for inflow,  $\Delta S$ , outflow and a column describing if the estimate is a “nowcast” or “forecast”. The user is also presented with three rows of inputs, corresponding to the next 3 anticipated satellite observation dates, where the expected storage change as a percentage of the maximum storage of the reservoir can be passed. The plot showing the  $\Delta S$  and outflow will then update, based on the choice of  $\Delta S$ , with the forecasted outflows highlighted as orange circles.

## 5. Conclusion

Regulation of rivers, and the issues associated with it, such as environmental degradation, conflicts among nations, and change in the river geomorphology are negatively affecting an increasing portion of the world. With a near-global coverage, publicly accessible methods and open-source code, and a record of reservoir operation dynamics, RAT 1.0 (Biswas et al., 2021) provided information on reservoir operation dynamics for understanding these increasingly regulated river systems.

Building on RAT 1.0, we made several improvements, based on stakeholder feedback, to develop a more skillful version 2.0 of the RAT framework. While these improvements were demonstrated using the Mekong River basin as an example, the newly developed framework can

apply anywhere where reservoirs need to be monitored routinely. Using techniques such as, advanced unsupervised classification-based water area estimation, an ensemble of sensors with complementing strengths, and a tiered filtering and correction approach, we were able to estimate changes in the reservoir dynamics with higher accuracies than RAT 1.0. This method, called the TMS-OS, was found to be highly skillful in quantifying the storage change, with a higher average correlation, and lower RMSE and MAE values as compared to RAT 1.0. This bodes well for the Surface Water and Ocean Topography (SWOT) mission (<https://swot.jpl.nasa.gov/>) which is planned for launch in 2022. The SWOT satellite mission is a joint mission of the National Aeronautics and Space Administration (NASA) and Center National d'Etudes Spatiales (CNES), with contributions from the Canada Space Agency and the United Kingdom Space Agency (Biancamaria et al., 2016). SWOT is expected to monitor reservoir elevation and extent at a global scale using its wide-swath capability (Lee et al., 2010) and thereby complement altimeters that have limited but accurate spatial sampling. The SWOT mission is therefore expected to further improve our ability to predict the dynamic state of reservoirs.

In general, RAT 2.0, with its use of multiple sensors and tiered methodologies, performed better than RAT 1.0 in characterizing the outflow from reservoirs. The ability of visualize the forecasted outflow, based on forecasted inflow and forecasted storage change, either from historical reservoir operation patterns, or expectation of dam operators based on human understanding, was also introduced in RAT 2.0.

Even though significant strides were made in quantification of the reservoir operation dynamics, there is always room for improvement. The effect of upstream reservoir operations on the downstream reservoirs remains to be taken into account and studied at the basin level. With the use of a greater suite of altimeters and sensors, combined with machine learning to automatically fill in inter-sensor gaps or data outages, we believe it may be possible to predict reservoir states consistently at the daily resolution, leading to higher accuracy in outflow estimation. Such future improvements can further help democratize the access to information on operations of dams towards more sustainable and equitable management of water resources.

**Software Availability:** [https://github.com/pritam47/rat\\_v2](https://github.com/pritam47/rat_v2).

#### Declaration of competing interest

The authors declare that they have no known competing financial interests or personal relationships that could have appeared to influence the work reported in this paper.

#### Data availability

In-situ reservoir operation data is available at <http://app.rid.gov.th:88/reservoir/>. The code can be accessed at [https://github.com/pritam47/rat\\_v2](https://github.com/pritam47/rat_v2). Other datasets used are freely accessible.

#### Acknowledgement

This study was supported by grant 80NSSC20k0152 from NASA titled “Operational Services for Water, Disaster and Hydropower Application for Lower Mekong Populations Using NASA Earth Observations and Models”. Additional support from NASA grant 80NSSC22K0918 titled “Improved Reservoir Management with Simultaneous Monitoring of Water Quantity and Quality using Multiple Satellites, SWOT and RAT-WQ2” is also gratefully acknowledged.

Appendix

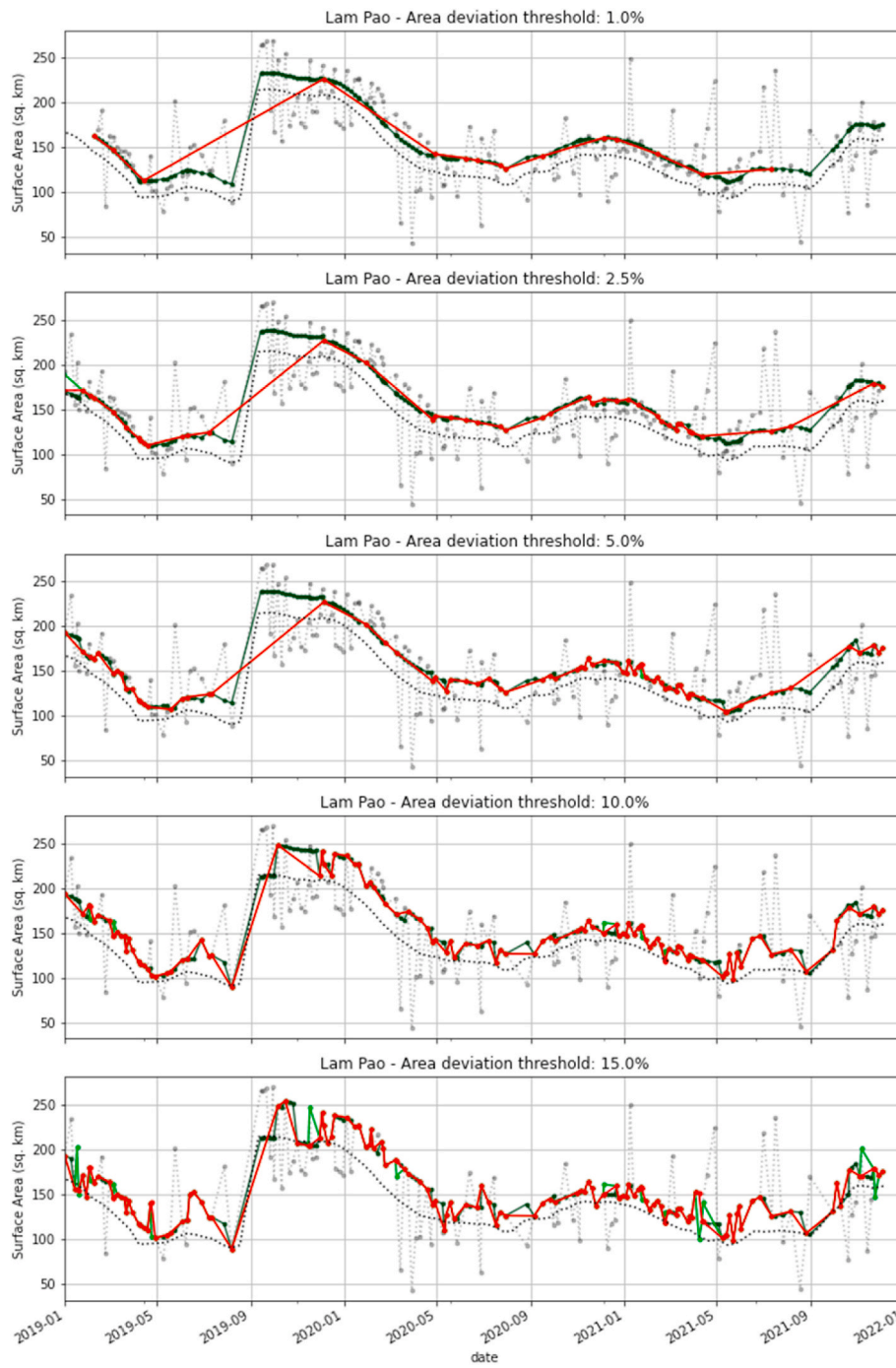


Fig. A.1. Effect of the choice of filtering 1 threshold on the surface area time-series – Lam Pao.

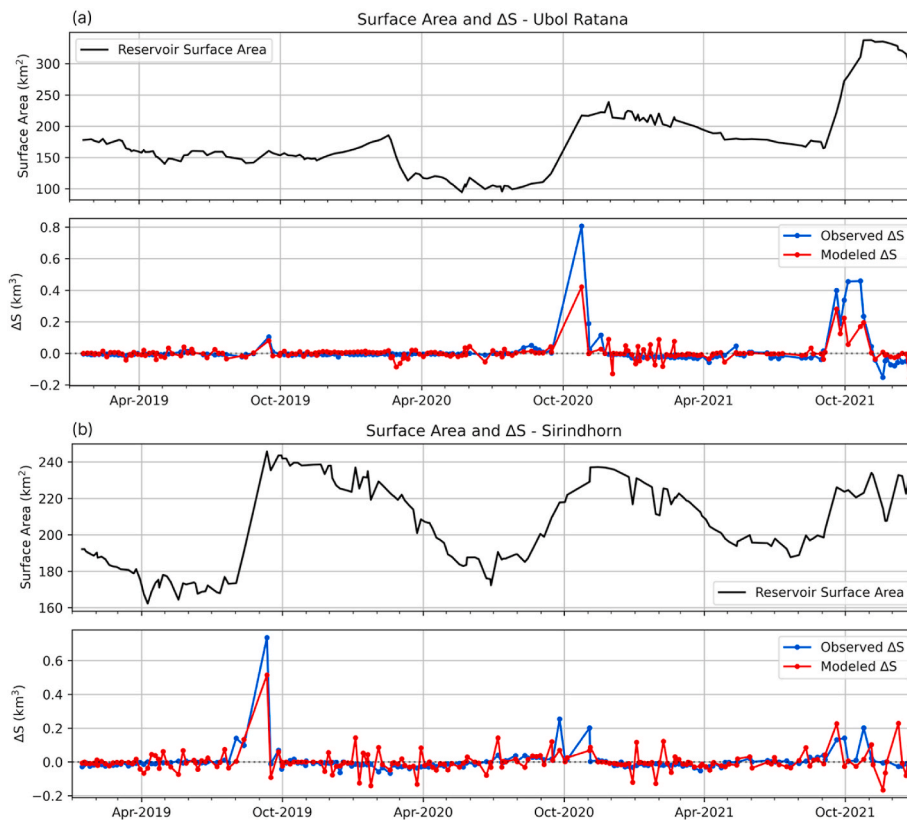


Fig. A.2. Comparison of modeled storage change with observed storage change for the three validation reservoirs. (a)  $\Delta S$  for Sirindhorn, (b)  $\Delta S$  for Ubol Ratana.

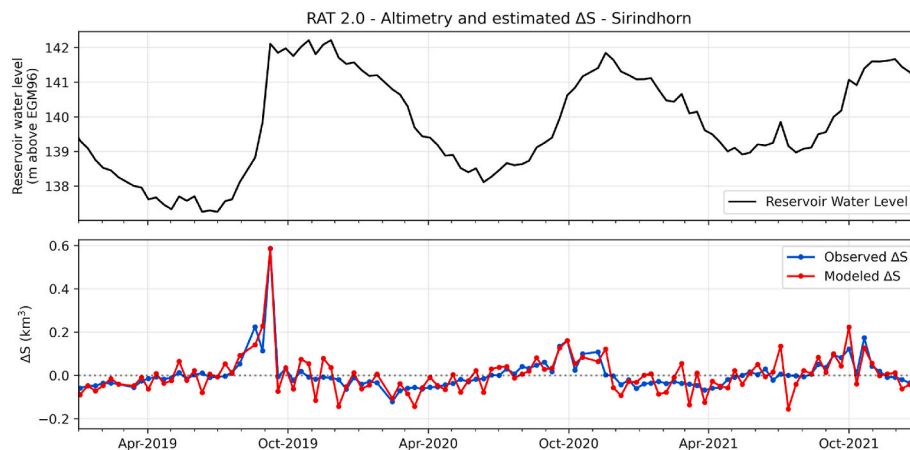


Fig. A.3. Comparison of modeled storage change using altimetry measurement of reservoir water level with observed storage change for Sirindhorn, Thailand.

References

Ahmad, S.K., Hossain, F., Eldardiry, H., Pavelsky, T.M., 2020. A fusion approach for water area classification using visible, near infrared and synthetic aperture radar for South Asian conditions. *IEEE Trans. Geosci. Rem. Sens.* 58 (4), 2471–2480. <https://doi.org/10.1109/TGRS.2019.2950705>.

Arias, M.E., Cochrane, T.A., Piman, T., Kummur, M., Caruso, B.S., Killeen, T.J., 2012. Quantifying changes in flooding and habitats in the Tonle Sap Lake (Cambodia) caused by water infrastructure development and climate change in the Mekong Basin. *J. Environ. Manag.* 112, 53–66. <https://doi.org/10.1016/j.jenvman.2012.07.003>.

Bakker, M.H.N., 2009. transboundary river floods and institutional capacity. *JAWRA Journal of the American Water Resources Association* 45 (3), 553–566. <https://doi.org/10.1111/j.1752-1688.2009.00325.x>.

Balthrop, C., Hossain, F., 2010. Short note: a review of state of the art on treaties in relation to management of transboundary flooding in international river basins and

the Global Precipitation Measurement mission. *Water Pol.* 12 (5), 635–640. <https://doi.org/10.2166/wp.2009.117>.

Barbarossa, V., Schmitt, R.J.P., Huijbregts, M.A.J., Zarfl, C., King, H., Schipper, A.M., 2020. Impacts of current and future large dams on the geographic range connectivity of freshwater fish worldwide. *Proc. Natl. Acad. Sci. USA* 117 (7), 3648–3655. <https://doi.org/10.1073/pnas.1912776117>.

Bennett, A., Hamman, J., Nijssen, B., 2020. MetSim: a Python package for estimation and disaggregation of meteorological data. *J. Open Source Software* 5 (47), 2042. <https://doi.org/10.21105/joss.02042>.

Bernaer, T., Böhmelt, T., 2020. International conflict and cooperation over freshwater resources. *Nat. Sustain.* 3 (5), 350–356. <https://doi.org/10.1038/s41893-020-0479-8>.

Birkett, C.M., Reynolds, C.A., Deeb, E.J., Ricko, M., Beckley, B.D., Yang, X., 2018, December 14. G-REALM: A Lake/Reservoir Monitoring Tool for Water Resources and Regional Security Assessment. AGU Fall Meeting, 2018. <https://agu.confex.com/agu/fm18/meetingapp.cgi/Paper/374138>.

- Biswas, N.K., Hossain, F., Bonnema, M., Lee, H., Chishtie, F., 2021. Towards a global Reservoir Assessment Tool for predicting hydrologic impacts and operating patterns of existing and planned reservoirs. *Environ. Model. Software* 140, 105043. <https://doi.org/10.1016/j.envsoft.2021.105043>.
- Bonnema, M., Hossain, F., 2017. Inferring reservoir operating patterns across the Mekong Basin using only space observations. *Water Resour. Res.* 53 (5), 3791–3810. <https://doi.org/10.1002/2016WR019978>.
- Bonnema, M., Sikder, S., Miao, Y., Chen, X., Hossain, F., Ara Pervin, I., Mahbubur Rahman, S.M., Lee, H., 2016. Understanding satellite-based monthly-to-seasonal reservoir outflow estimation as a function of hydrologic controls: satellite-based reservoir outflow. *Water Resour. Res.* 52 (5), 4095–4115. <https://doi.org/10.1002/2015WR017830>.
- Calinski, T., Harabasz, J., 1974. A dendrite method for cluster analysis. *Commun. Stat. Theor. Methods* 3 (1), 1–27. <https://doi.org/10.1080/03610927408827101>.
- Cooley, S.W., Ryan, J.C., Smith, L.C., 2021. Human alteration of global surface water storage variability. *Nature* 591 (7848), 78–81. <https://doi.org/10.1038/s41586-021-03262-3>.
- Cordeiro, M.C.R., Martinez, J.-M., Peña-Luque, S., 2021. Automatic water detection from multidimensional hierarchical clustering for Sentinel-2 images and a comparison with Level 2A processors. *Rem. Sens. Environ.* 253, 112209. <https://doi.org/10.1016/j.rse.2020.112209>.
- Dac Tran, D., Thi Nguyen, V., Thi My To, H., Trung Nguyen, T., Minh Dinh, Q., 2020. Species composition and biodiversity index of gobiid assemblage in estuarine areas of the Mekong Delta, Vietnam. *Egypt. J. Aquat. Biol. Fish.* 24 (7-Special issue), 931–941. <https://doi.org/10.21608/ejafb.2020.131385>.
- Dingman, S.L., 2015. *Physical Hydrology*, third ed. Waveland Press, Inc.
- Earth Resources Observation And Science (EOS) Center, 2017. *Shuttle Radar Topography Mission (SRTM) 1 Arc-Second Global* [Tiff]. U.S. Geological Survey. <https://doi.org/10.5066/F7PR7TFT>.
- EGAT, 2019. *The Study of Probable Maximum Flood and Spillway Operation for Dam Safety of EGAT's Dam*. Electricity Generating Authority of Thailand, Ministry of Energy.
- Eldardiry, H., Hossain, F., 2019. Understanding reservoir operating rules in the transboundary Nile River basin using macroscale hydrologic modeling with satellite measurements. *J. Hydrometeorol.* 20 (11), 2253–2269. <https://doi.org/10.1175/JHM-D-19-0058.1>.
- Eldardiry, H., Hossain, F., 2021a. The value of long-term streamflow forecasts in adaptive reservoir operation: the case of the high aswan dam in the transboundary Nile River basin. *J. Hydrometeorol.* 22 (5), 1099–1115. <https://doi.org/10.1175/JHM-D-20-0241.1>.
- Eldardiry, H., Hossain, F., 2021b. A blueprint for adapting high Aswan dam operation in Egypt to challenges of filling and operation of the Grand Ethiopian Renaissance dam. *J. Hydrol.* 598, 125708. <https://doi.org/10.1016/j.jhydrol.2020.125708>.
- Fernandes, M.R., Aguiar, F.C., Martins, M.J., Rivaes, R., Ferreira, M.T., 2020. Long-term human-generated alterations of Tagus River: effects of hydrological regulation and land-use changes in distinct river zones. *Catena* 188, 104466. <https://doi.org/10.1016/j.catena.2020.104466>.
- Google, 2022, March 10. *Ee.Clusterer.wekaCascadeKMeans* | Google Earth Engine. Google Developers. <https://developers.google.com/earth-engine/apidocs/ee-clusterer-wekacascadekmeans>.
- Grill, G., Lehner, B., Lumsdon, A.E., MacDonald, G.K., Zarfl, C., Reidy Liermann, C., 2015. An index-based framework for assessing patterns and trends in river fragmentation and flow regulation by global dams at multiple scales. *Environ. Res. Lett.* 10 (1), 015001. <https://doi.org/10.1088/1748-9326/10/1/015001>.
- Gupta, H.V., Kling, H., Yilmaz, K.K., Martinez, G.F., 2009. Decomposition of the mean squared error and NSE performance criteria: implications for improving hydrological modelling. *J. Hydrol.* 377 (1–2), 80–91. <https://doi.org/10.1016/j.jhydrol.2009.08.003>.
- Hamman, J., Nijssen, B., 2016. Vic: Vic 4.2. D. Zenodo. <https://doi.org/10.5281/ZENODO.56057>.
- Hamman, J., Nijssen, B., Bohn, T., Gergel, D., Franssen, W., Homefc, Yixin Mao, Helgason, Hordur, Suzuki, K., Rk, M., Badger, T.G., Craig, T., Zwart, J., Kiritokun07, Peng, B., 2021. *UW-Hydro/VIC: VIC 5.1.0* (5.1.0). Zenodo. <https://doi.org/10.5281/ZENODO.5781377>.
- Hamman, J., Nijssen, B., Bohn, T.J., Gergel, D.R., Mao, Y., 2018. The Variable Infiltration Capacity model version 5 (VIC-5): infrastructure improvements for new applications and reproducibility. *Geosci. Model Dev. (GMD)* 11 (8), 3481–3496. <https://doi.org/10.5194/gmd-11-3481-2018>.
- Hanasaki, N., Kanae, S., Oki, T., 2006. A reservoir operation scheme for global river routing models. *J. Hydrol.* 327 (1–2), 22–41. <https://doi.org/10.1016/j.jhydrol.2005.11.011>.
- Harbeck, G.E., 1962. *A Practical Field Technique for Measuring Reservoir Evaporation Utilizing Mass-Transfer Theory* (Studies of Evaporation. U.S. Department of the Interior [Geological Survey Professional Paper 272-E]).
- Hossain, F., Sikder, S., Biswas, N., Bonnema, M., Lee, H., Luong, N.D., Hiep, N.H., Du Duong, B., Long, D., 2017. Predicting water availability of the regulated Mekong river basin using satellite observations and a physical model. *Asian J. Water Environ. Pollut.* 14 (3), 39–48. <https://doi.org/10.3233/AJW-170024>.
- Khandekar, N., Srinivasan, V., 2021. Dispute resolution in the Cauvery basin, India. In: Ferrier, R., Jenkins, A. (Eds.), *Handbook of Catchment Management* 2e, first ed. Wiley, pp. 549–577. <https://doi.org/10.1002/9781119531241.ch22>.
- Knoben, W.J.M., Freer, J.E., Woods, R.A., 2019. Technical note: inherent benchmark or not? Comparing nash-sutcliffe and kling-Gupta efficiency scores [Preprint]. *Catchment Hydrol./Model. Approaches*. <https://doi.org/10.5194/hess-2019-327>.
- Kondolf, G.M., Schmitt, R.J.P., Carling, P., Darby, S., Arias, M., Bizzi, S., Castelletti, A., Cochrane, T.A., Gibson, S., Kumm, M., Oeurng, C., Rubin, Z., Wild, T., 2018. Changing sediment budget of the Mekong: cumulative threats and management strategies for a large river basin. *Sci. Total Environ.* 625, 114–134. <https://doi.org/10.1016/j.scitotenv.2017.11.361>.
- Lee, H., Durand, M., Jung, H.C., Alsdorf, D., Shum, C.K., Sheng, Y., 2010. Characterization of surface water storage changes in Arctic lakes using simulated SWOT measurements. *Int. J. Rem. Sens.* 31 (14), 3931–3953. <https://doi.org/10.1080/01431161.2010.483494>.
- Lehner, B., Liermann, C.R., Revenga, C., Vörösmarty, C., Fekete, B., Crouzet, P., Doll, P., Endejan, M., Frenken, K., Magome, J., Nilsson, C., Robertson, J.C., Rödel, R., Sindorf, N., Wisser, D., 2011. High-resolution mapping of the world's reservoirs and dams for sustainable river-flow management. *Front. Ecol. Environ.* 9 (9), 494–502. <https://doi.org/10.1890/100125>.
- Li, S., Xu, Y.J., Ni, M., 2021. Changes in sediment, nutrients and major ions in the world largest reservoir: effects of damming and reservoir operation. *J. Clean. Prod.* 318, 128601. <https://doi.org/10.1016/j.jclepro.2021.128601>.
- Lohmann, D., Raschke, E., Nijssen, B., Lettenmaier, D.P., 1998. Regional scale hydrology: I. Formulation of the VIC-2L model coupled to a routing model. *Hydrol. Sci. J.* 43 (1), 131–141. <https://doi.org/10.1080/02626669809492107>.
- Mekong River Commission, 2019. State of the Basin Report 2018. Mekong River Commission. [https://www.mrcmekong.org/assets/Publications/SOBR-v8\\_Final-f0r-web.pdf](https://www.mrcmekong.org/assets/Publications/SOBR-v8_Final-f0r-web.pdf).
- Mekong River Commission, 2021. The Integrated Water Resources Management-Based Basin Development Strategy for the Lower Mekong Basin 2021–2030 and the MRC Strategic Plan 2021–2025. <https://www.mrcmekong.org/assets/Publications/BDS-2021-2030-and-MRC-SP-2021-2025.pdf>.
- Mulligan, M., van Soesbergen, A., Sáenz, L., 2020. GOODD, a global dataset of more than 38,000 georeferenced dams. *Sci. Data* 7 (1), 31. <https://doi.org/10.1038/s41597-020-0362-5>.
- National Centers For Environmental Prediction/National Weather Service/NOAA/U.S. Department Of Commerce, 2015. NCEP GFS 0.25 Degree Global Forecast Grids Historical Archive. UCAR/NCAR - Research Data Archive. <https://doi.org/10.5065/D65D8PWK>. <https://rda.ucar.edu/datasets/ds084.1/#!description>. (Accessed 28 March 2022).
- Okeowo, M.A., Lee, H., Hossain, F., Getirana, A., 2017. Automated generation of lakes and reservoirs water elevation changes from satellite radar altimetry. *IEEE J. Sel. Top. Appl. Earth Obs. Rem. Sens.* 10 (8), 3465–3481. <https://doi.org/10.1109/JSTARS.2017.2684081>.
- Pekel, J.-F., Cottam, A., Gorelick, N., Belward, A.S., 2016. High-resolution mapping of global surface water and its long-term changes. *Nature* 540 (7633), 418–422. <https://doi.org/10.1038/nature20584>.
- Penman, H.L., 1948. Natural evaporation from open water, bare soil and grass. *Proc. Roy. Soc. Lond. Math. Phys. Sci.* 193 (1032), 120–145. <https://doi.org/10.1098/rspa.1948.0037>.
- Plengsaeng, B., Wehn, U., van der Zaag, P., 2014. Data-sharing bottlenecks in transboundary integrated water resources management: a case study of the Mekong River Commission's procedures for data sharing in the Thai context. *Water Int.* 39 (7), 933–951. <https://doi.org/10.1080/02508060.2015.981783>.
- Pokhrel, Y., Shin, S., Lin, Z., Yamazaki, D., Qi, J., 2018. Potential disruption of flood dynamics in the lower Mekong river basin due to upstream flow regulation. *Sci. Rep.* 8 (1), 17767. <https://doi.org/10.1038/s41598-018-35823-4>.
- RID, 2022. Reservoir monitoring system for Thailand. Retrieved March 31, 2022, from. <https://app.rid.go.th:88/reservoir/>.
- Ryan, J.C., Smith, L.C., Cooley, S.W., Pitcher, L.H., Pavelsky, T.M., 2020. Global characterization of inland water reservoirs using ICESat-2 altimetry and climate reanalysis. *Geophys. Res. Lett.* 47 (17), e2020GL088543. <https://doi.org/10.1029/2020GL088543>.
- Valbo-Jørgensen, J., Coates, D., Hortle, K., 2009. Fish diversity in the Mekong river basin. In: *The Mekong*. Elsevier, pp. 161–196. <https://doi.org/10.1016/B978-0-12-374026-7.00008-5>.
- Van Bavel, C.H.M., 1966. Potential evaporation: the combination concept and its experimental verification. *Water Resour. Res.* 2 (3), 455–467. <https://doi.org/10.1029/WR002i003p00455>.
- Wang, X., Xie, S., Zhang, X., Chen, C., Guo, H., Du, J., Duan, Z., 2018. A robust Multi-Band Water Index (MBWI) for automated extraction of surface water from Landsat 8 OLI imagery. *Int. J. Appl. Earth Obs. Geoinf.* 68, 73–91. <https://doi.org/10.1016/j.jag.2018.01.018>.
- Wu, H., Kimball, J.S., Mantua, N., Stanford, J., 2011. Automated upscaling of river networks for macroscale hydrological modeling: upscaling of global river networks. *Water Resour. Res.* 47 (3). <https://doi.org/10.1029/2009WR008871>.
- Zhao, G., Gao, H., 2018. Automatic correction of contaminated images for assessment of reservoir surface area dynamics. *Geophys. Res. Lett.* <https://doi.org/10.1029/2018GL078343>.
- Zhou, T., Nijssen, B., Gao, H., Lettenmaier, D.P., 2016. The contribution of reservoirs to global land surface water storage variations. *J. Hydrometeorol.* 17 (1), 309–325. <https://doi.org/10.1175/JHM-D-15-0002.1>.
- Ziv, G., Baran, E., Nam, S., Rodríguez-Iturbe, I., Levin, S.A., 2012. Trading-off fish biodiversity, food security, and hydropower in the Mekong River Basin. *Proc. Natl. Acad. Sci. USA* 109 (15), 5609–5614. <https://doi.org/10.1073/pnas.1201423109>.